International Journal of Thermal Sciences 48 (2009) 1564–1573

Contents lists available at ScienceDirect

International Journal of Thermal Sciences

www.elsevier.com/locate/ijts

Flow over porous blocks in a square cavity: Influence of heat flux and porosity on heat transfer rates

S.Z. Shuja [a], B.S. Yilbas [a,*], M. Kassas [b]

[a] Mechanical Engineering Department, KFUPM, Dhahran 31261, Saudi Arabia
[b] Electrical Engineering Department, KFUPM, Dhahran 31261, Saudi Arabia

ARTICLE INFO

Article history:
Received 4 June 2008
Received in revised form 10 December 2008
Accepted 14 December 2008
Available online 15 January 2009

Keywords:
Porous
Blocks
Cavity
Flow
Heat transfer

ABSTRACT

The heat transfer due to the flow over two porous blocks situated in a square cavity is investigated and the effects of heat flux and the porosity on the flow structure and the heat transfer in the cavity are examined. In the simulations, four heat fluxes and three porosities are accommodated while air is used as the working fluid. The flow conditions at the cavity inlet are kept the same for all the cases simulated. The equilibrium equations pertinent to the flow over porous blocks in the cavity are used to predict the velocity and temperature fields. It is found that increasing porosity of the blocks modifies the flow field in the cavity, which is more pronounced as the heat flux increases. The Nusselt number enhances with the increasing porosity and heat flux.

1. Introduction

The porous structures are widely used to improve the heat transfer rates in the flow systems. In this case, the porous structures are situated in and around the heat generating bodies subjected to convection cooling. In some of the cooling applications, the porous structures are situated in an open-end cavity and the flow passes over the porous blocks. The orientation and the aspect ratios of the porous blocks become important for enhance the heat transfer rates while lowering the fluid power losses in the cavity. Consequently, investigation into the flow structure and heat transfer characteristics in the flow system consisting of cavity and heat generating porous blocks become essential.

Considerable research studies were carried out to examine the flow over porous blocks. A semi-empirical model for the permeability and the inertial coefficient of fin-fin heat sinks was introduced by Jeng and Tzeng [1]. They showed that the model introduced predicted results comparable to the data obtained for the experimental study. The numerical approach for a steady flow and heat transfer in the separation region of the embedded porous media was introduced by Hassanien et al. [2]. They simplified the boundary layer equations to semi-similar equations and used the local non-similarity method with the second order truncation to predict the flow properties and heat transfer characteristics. The heat transfer in a porous channel subjected to an oscillating flow was studied experimentally by Fu et al. [3]. They showed that the flow oscillation enhanced the heat transfer rates and could be considered as an effective method for cooling high speed electronic devices. The free convection from a vertical plate fin with a rounded tip imbedded in a porous medium was investigated by Vaszi et al. [4]. They showed that increasing the heat transferring surface did not enhance the total heat transfer; however, fin aspect ratio and convection-conduction heat transfer parameter influenced the total heat transfer rates. Heat transfer and fluid flow in porous carbon foam were examined by Yu et al. [5]. They indicated that the fluid pressure drop was well described by Darcy–Forchhiemer law. The fluid flow and the heat transfer in liquid cooled porous heat sinks were examined by Zhang et al. [6]. They showed that the thermal resistances for foam heat sinks decreased with increased in flow rate and attained their minimum at their highest flow rates, whereas the pressure drop increased more rapidly with the increasing mass flow rate. The non-Darcy natural convection in high porosity metal foams was considered by Phanikumar and Mahajan [7]. They indicated that the thermal non-equilibrium model provided superior description of the heat transfer in metal foams, especially in the presence of the fluid-porous interfaces. The characteristics of oscillating flow through a channel filled with open-cell metal foam were investigated by Leong and Jin [8]. They showed that the flow characteristics were governed by the Reynolds number based on the hydraulic ligament diameter. Natural convection heat transfer form a vertical cylindrical porous fin was examined numerically by Naidu et al. [9]. They indicated that increasing permeability of the porous foam resulted in decrease of the fin temperature as well as the fin efficiency. The

* Corresponding author.
E-mail address: bsyilbas@kfupm.edu.sa (B.S. Yilbas).

1290-0729/$ – see front matter
doi:10.1016/j.ijthermalsci.2008.12.010

Nomenclature

A	area	m^2	
C_1	inertial resistance factor		
g	center of gravity	m/s^2	
Gr	Grashoff number		
E_f	fluid energy	J/kg	
E_s	solid medium energy	J/kg	
h	heat transfer coefficient	$W/m^2\,K$	
$\bar{h}$	averaged heat transfer coefficient	$W/m^2\,K$	
K	permeability of porous block		
k_f	thermal conductivity of fluid	W/m K	
k_s	thermal conductivity of solid	W/m K	
k_{eff}	effective thermal conductivity	W/m K	
L	cavity length	m	
f	inertia coefficient		
F	body force	N	
L	width of channel	m	
n	any spatial coordinate		
Nu	Nuselt number		
p	pressure	Pa	
q	heat transfer rate	W	
$\dot{q}$	rate of heat generation per unit volume	W/m^3	
S_f^k	fluid enthalpy source term	W/m^3	
T	temperature	K	
T_{avg}	average temperature	K	
T_i	cavity inlet temperature	K	
T_s	surface temperature	K	
u	velocity in x-axis	m	
U_i	mean velocity at block inlet	m/s	
v	velocity in y-axis	m	
V	velocity vector		
x	distance in x-axis	m	
y	distance in y-axis	m	
α	the coefficient in the viscous loss term		
β	volumetric thermal expansion coefficient	1/K	
ε	porosity		
φ	any property of fluid		
τ	shear stress	N/m^2	
μ	viscosity	$N\,s/m^3$	
υ	kinematic viscosity	m^2/s	
ρ	density	kg/m^3	
$\forall$	volume of the block	m^3	

flow structure and heat transfer within a cellular copper structures were investigated by Tian et al. [10]. They indicated that the overall heat transfer depended on the porosity and the surface area of the copper structure. The flow and heat transfer in porous channel with the solid baffles were studied by Nicolau et al. [11]. They indicated that no advantages were observed when using the low porosity baffles in the laminar flow regime in the channel. The thermal performance of a graphite foam evaporator and its potential use in the thermal management of electronic devices were examined by Coursey et al. [12]. They showed that using the graphite foam as the evaporator enabled the transfer of large amount of energy with relatively low temperature difference and without the need for external pumping. The thermal characterization of carbon foams in parallel flow was studied by Straatman et al. [13]. They indicated that the heat transfer was independent of the effective conductivity considered in the experiments.

The porous structures are widely used in electronic device cooling applications [14]. This is because of the achievement of high cooling rates. Moreover, the porosity and heat flux are the two of the important parameters influencing the flow structure and heat transfer rates around the heat transferring bodies. Consequently, investigation into the influence of porosity and heat flux on the heat transfer rates becomes crucial. In the present study, the heat transfer from two porous blocks situated in a square cavity is considered. A laminar air flow is introduced at the cavity inlet while the constant heat flux is employed in the porous structures. To examine the effects of porosity and amount of heat flux on the flow structure and the heat transfer rates, three porosities of the blocks and four levels of heat fluxes are accommodated in the simulations.

2. Mathematical analysis

The equations governing the flow over a porous block situated in a channel can be formulated through considering the equilibrium conditions. In this case, porous medium can be defined as a material consisting of a solid matrix with an interconnected void and it is assumed that a single fluid (single phase) occupies the voids spaces. Moreover, assuming isotopic porosity and single phase steady flow, the volume-averaged mass and momentum conservation equations for a steady flow situation can be written in vector notation as:

$$\nabla \cdot (\varepsilon \rho V) = 0 \tag{1}$$

and

$$\nabla \cdot (\varepsilon \rho V V) = -\varepsilon \nabla p + \nabla \cdot (\varepsilon \tau) + \varepsilon F - \left(\frac{\mu}{\alpha} + \frac{C_1 \rho}{2}|V|\right)V \tag{2}$$

The last term in this equation represents the viscous (Darcy loss term) and inertial drag forces imposed by the pore walls on the fluid. Note that ε is the porosity of the media defined as the ratio of the volume occupied by the fluid to the total volume. However, the term $(\frac{\mu}{\alpha} + \frac{C_1\rho}{2}|V|)V$ in Eq. (2) is the source term due to the porous media. However, outside of the porous media, the source term drops and $\varepsilon = 1$. Therefore, Eq. (2) reduces to the standard momentum equation for a single phase steady fluid flow. The coefficient α in the viscous loss term equals to K, permeability of the porous structure. The coefficient C_1 in the inertial loss term is written as:

$$C_1 = \frac{f}{\sqrt{K}}$$

f is the inertia coefficient reflecting porous inertia effects. However, K and f are related to structure of the porous medium as given by Battacharya et al. [15]. The values of K and f are given in Table 1 for two porous blocks.

Table 1
Properties of porous blocks used in the simulations.

Porosity (ε)	f	K ($\times 10^7$ m^2)
0.9726	0.097	2.7
0.8991	0.068	0.94

The standard energy transport equation in porous media regions is solved with modifications to the conduction flux and the transient terms only. In the porous medium, the conduction flux

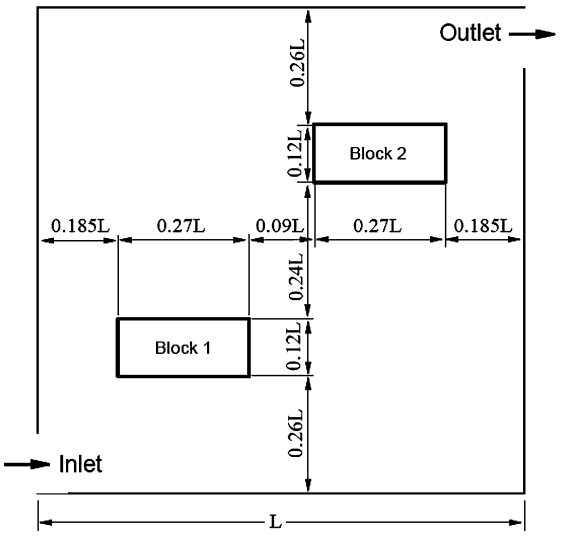

Fig. 1. View of cavity and solid blocks in the cavity. Blocks configuration in the cavity for the block aspect ratio of 2.25 and $L = 0.05$ m.

uses an effective conductivity and the transient terms includes the thermal inertia of the solid region on the medium

$$\nabla \cdot \left(V(\rho_f E_f + P)\right) = \nabla \cdot (k_{\text{eff}} \nabla T - \tau \cdot V) + S_f^k \tag{3}$$

where the effective thermal conductivity in the porous medium, k_{eff}, is the volume average of the fluid conductivity and the solid conductivity.

$$k_{\text{eff}} = \varepsilon k_f + (1 - \varepsilon) k_s \tag{4}$$

where E_f is the fluid energy per unit mass, k_f is the fluid phase thermal conductivity (including the turbulent contribution (k_t), k_s is the solid medium thermal conductivity, k_{eff} is the effective thermal conductivity of the medium, S_f^k is the fluid enthalpy source term, ε is the porosity of the medium, V is the velocity vector, τ is shear stress, P is the pressure, and F is the body force including that due to buoyancy.

In the case of fluid side, the governing equations of flow are modified, and ε in Eqs. (1), (2) and (3) is set to 1. In addition, k_{eff} is becomes k_f (fluid thermal conductivity) in Eq. (4).

2.1. Fluid and solid blocks boundary conditions

Two solid blocks with different geometric arrangements in open-ends cavity is considered. The square blocks are accommodated and the surface area of each block is kept the same. Fig. 1 shows the schematic view of the solution domain (cavity and the geometric configurations of the blocks) while Table 2 gives the geometric dimensions of the solution domain. The blocks are numbered in such away that the first block is defined as Block 1 and the second block is named as Block 2 in the cavity. The geometric arrangement of blocks in the cavity is named as configurations; therefore, four configurations of blocks in the cavity are employed in the simulations. Moreover, the velocity magnitude is normalized through diving it by the cavity inlet velocity.

The adiabatic cavity walls with no slip and impermeable wall conditions for the velocity components are considered, i.e.,

$$\frac{\partial T}{\partial n} = 0, \qquad u = v = 0 \tag{5}$$

The pressure boundary is assumed at cavity exit while the uniform flow and temperature are assumed at cavity inlet, i.e.,

$$\frac{\partial \varphi}{\partial n} = 0 \tag{6}$$

where φ is any property of the fluid.

Table 2
Block and cavity dimensions, and porosity used in the simulations.

Cavity length	L (0.05 m)
Cavity width	L (0.05 m)
Total area of each block	$(0.18L)^2$ (8.1×10^{-5} m^2)
Cavity inlet port size	$0.2L$ (0.01 m)
Cavity exit port size	$0.2L$ (0.01 m)
Cavity inlet velocity	0.1544 m/s
Re_{Inlet}	100
Rate of heat generation (q)	$(1, 2, 3, 4) \times 10^5$ W/m^3
Porosity for each block	0, 0.8991, 0.9726

Table 3
Properties of the fluid and solid block used in the simulations.

	Air	Solid block
Density (kg/m^3)	1.177	7836
Specific heat (J/kg K)	1005	969
Thermal conductivity (W/m K)	0.02565	28.2
Viscosity (m^2/s)	1.544×10^{-5}	–

The uniform heat generation (q) is introduced in the rectangular porous and solid blocks (reference to Fig. 1). The temperature and heat flux continuity are assumed at solid block-fluid interface, i.e.

$$T_s = T_f \quad \text{and} \quad k_s \left(\frac{dT}{dn}\right)_s = k_f \left(\frac{dT}{dn}\right)_f \tag{7}$$

Air is used as the flowing fluid while solid block is considered to be steel. The properties of air at standard pressure and temperature and thermal properties of block are given in Table 3.

The averaged heat transfer coefficient is determined from:

$$\bar{h} = \frac{q}{A \Delta T_{\text{avg}}} \tag{8}$$

where A is the cross sectional area of the porous media while ΔT_{avg} is the temperature difference between the average surface temperature of the porous media and the cavity inlet temperature. The Nusselt number is determined from:

$$Nu = \frac{\bar{h} L}{k_{\text{eff}}} \tag{9}$$

where L is the wetted perimeter of the heated section of the porous media. The Grashoff number is defined by:

$$Gr = \frac{g\beta(T_s - T_i)L^3}{\nu^2} \tag{10}$$

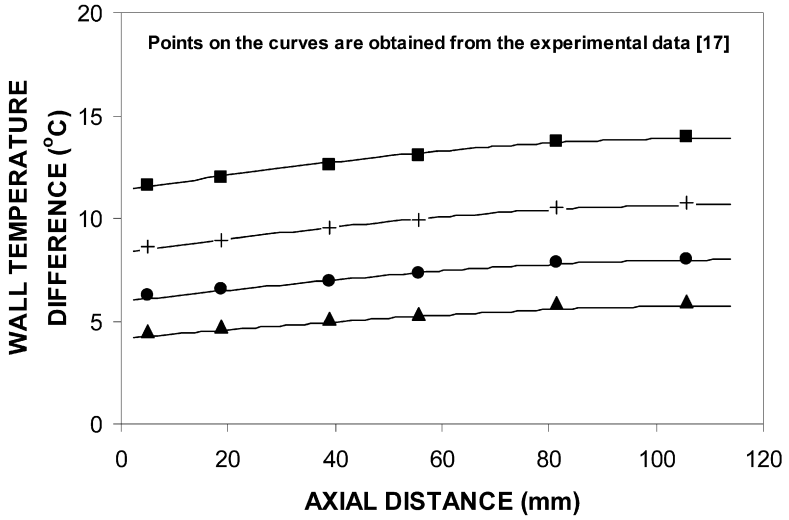

Fig. 2. Wall temperature difference predicted and obtained from the experimental data along the axial distance. The curves represent the predictions for different inlet average velocities while the dotted points are obtained from the experimental data [17] for different inlet averaged velocities.

Table 4
Metal foam characteristics used in the simulations.

Porosity (ε)	f	$K(\times 10^7\ \mathrm{m}^2)$
0.9118	0.085	1.8

where T_s is the average surface temperature of the porous media and L is the length of the porous block.

2.2. Numerical solution

The flow domain is overlaid with a rectangular grid as shown. The control volume approach is employed in the numerical scheme. All the variables are computed at each grid point except the velocities, which are determined midway between the grid points. The details of control volume approach are given by Patankar [16]. The grid independent tests are carried out and 192×192 grid size are selected on the basis of grid independent solutions with less computation time.

A staggered grid arrangement is used in the present study, which provides the pressure linkages through the continuity equation and is known as SIMPLE algorithm as presented by Patankar [16]. This procedure is an iterative process for convergence. The pressure link between continuity and momentum is established by transforming the continuity equation into a Poisson equation for pressure.

To simulate the flow field and heat transfer rates from the blocks, FLUENT code was used in relation to the numerical scheme and boundary conditions introduced in this study.

3. Model validation

The experiment carried out previously is simulated for the metal foam to validate the model study [17]. The simulation conditions are kept identical to the experimental parameters. In this case, a fully developed flow inlet to the duct partially filled with the metal foam with 63 mm $\times$ 45 mm $\times$ 114 mm size is considered. The characteristics of the metal foam are given in Table 4. The constant heat generation from the top and bottom walls of the duct is considered in consistent with the experimental study. Fig. 2 shows the predictions obtained from the model study and the experimental results. It can be observed that both results are in good agreement.

4. Results and discussion

Flow over porous blocks in a square cavity is considered and effects of heat flux and porosity of blocks on the flow structure and the heat transfer rates are examined. Air is considered as the working fluid in the cavity.

Fig. 3 shows normalized velocity (V/V_i) contours in the cavity for different heat fluxes and porosities. The influence of the porosity on the flow structure is more pronounced than that of the heat flux. Increasing porosity of the blocks allows fluid penetrating through the porous blocks and mixing with the convection current in the down stream of the blocks. However the natural convection current developed around the blocks contributes to the flow mixing in the cavity. This is more pronounced behind the blocks. The forced convection current is dominant in the region of the sides and below the blocks. However, the flow circulation in the region of the corners other than inlet and exit port, is not evident from the figure. In this case, the flow entering from the inlet port splits around the first block (Block 1, Fig. 1), and merges in the down stream of the block before under going the secondary splitting around the second block. Consequently, the forced convection current dominates in this region. In the region of the cavity exit port, the flow acceleration is evident, in which case, the pressure drop in this region is responsible for the flow acceleration. In addition, a small circulation cell is developed at the bottom corner of the first block. The size and the orientation of the circulation cell change with the magnitude of the heat flux. In the case of a solid block ($\varepsilon = 0$), flow circulation occurs on the left side of the block. This is caused by the flow splitting around the first block. Once the axial momentum in this region is reduced due to the shear layer developed around the solid block, the flow circulation is resulted. However, the effect of the heat flux on the flow structure in this region is not significant, i.e., the size and the orientation of the circulation cell remains almost the same at different magnitudes of the heat flux in the solid body.

Fig. 4 shows normalized temperature (T/T_i) contours in the cavity for different porosities and heat fluxes. The influence of the heat flux on the temperature field is significant. Increasing heat flux enhances the high temperature field above the first block (Block 1). This situation is more pronounced for the porous blocks. Increasing the porosity enhances the rate of flow penetrating through the porous blocks. Since temperature of the working fluid increases through the penetration, the high temperature region extends into the cavity. The natural convection current ema-

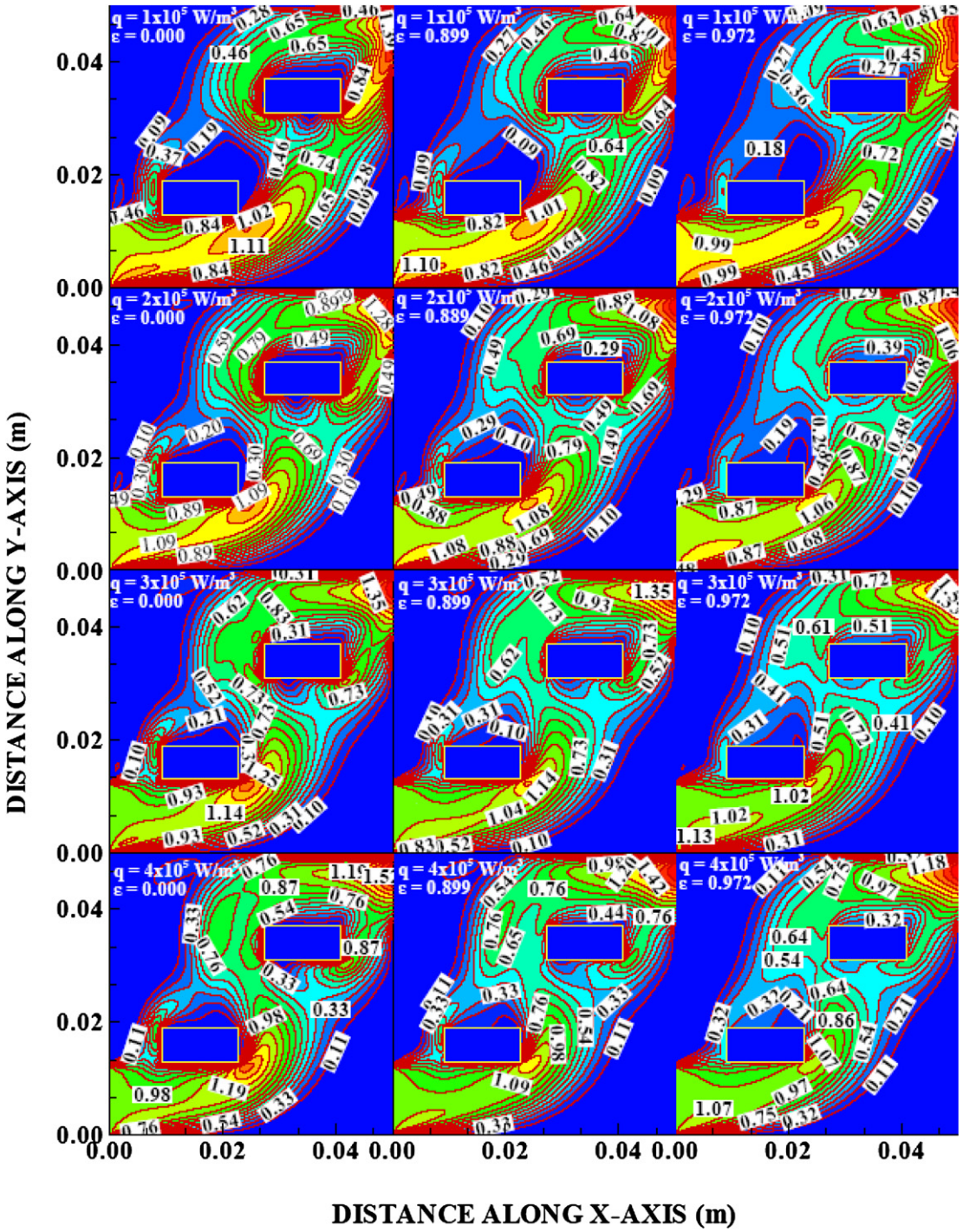

Fig. 3. Normalized velocity magnitude (V/V_i) contours in the cavity for different magnitude of heat flux and porosities.

nating from the heated porous blocks contributes to this extension. Moreover, in the region, where the forced convection current dominates in the cavity, low temperature region dominates in the cavity. This is because of the low temperature fluid entering into the cavity, which splits around the first block as well as the convective current passing below the cavity does not loose its axial momentum while accelerating towards the cavity exit. Consequently, low temperature fluid flow dominates in this region. In the case of the solid block, contribution of the natural convection current to the high temperature region, which is formed behind the blocks, is significant. Since, the solid blocks are at higher temperature than the fluid temperature, the thermal boundary layer developed around the block becomes thicker in the region where the forced convection current becomes ineffective. Consequently, the thickening of the thermal boundary layer contributes to the natural convection current and the extension of high temperature region in the cavity. This is more pronounced in the region above the first block, where the mixing of forced and natural convection currents are minimum in the cavity.

Fig. 5 shows contours of pressure coefficients in the cavity for different porosities and heat flux magnitudes. The pressure coefficient becomes less in the region where the forced and natural convection currents are high. Increasing porosity reduces the pressure coefficient behind the blocks, which is more pronounced for

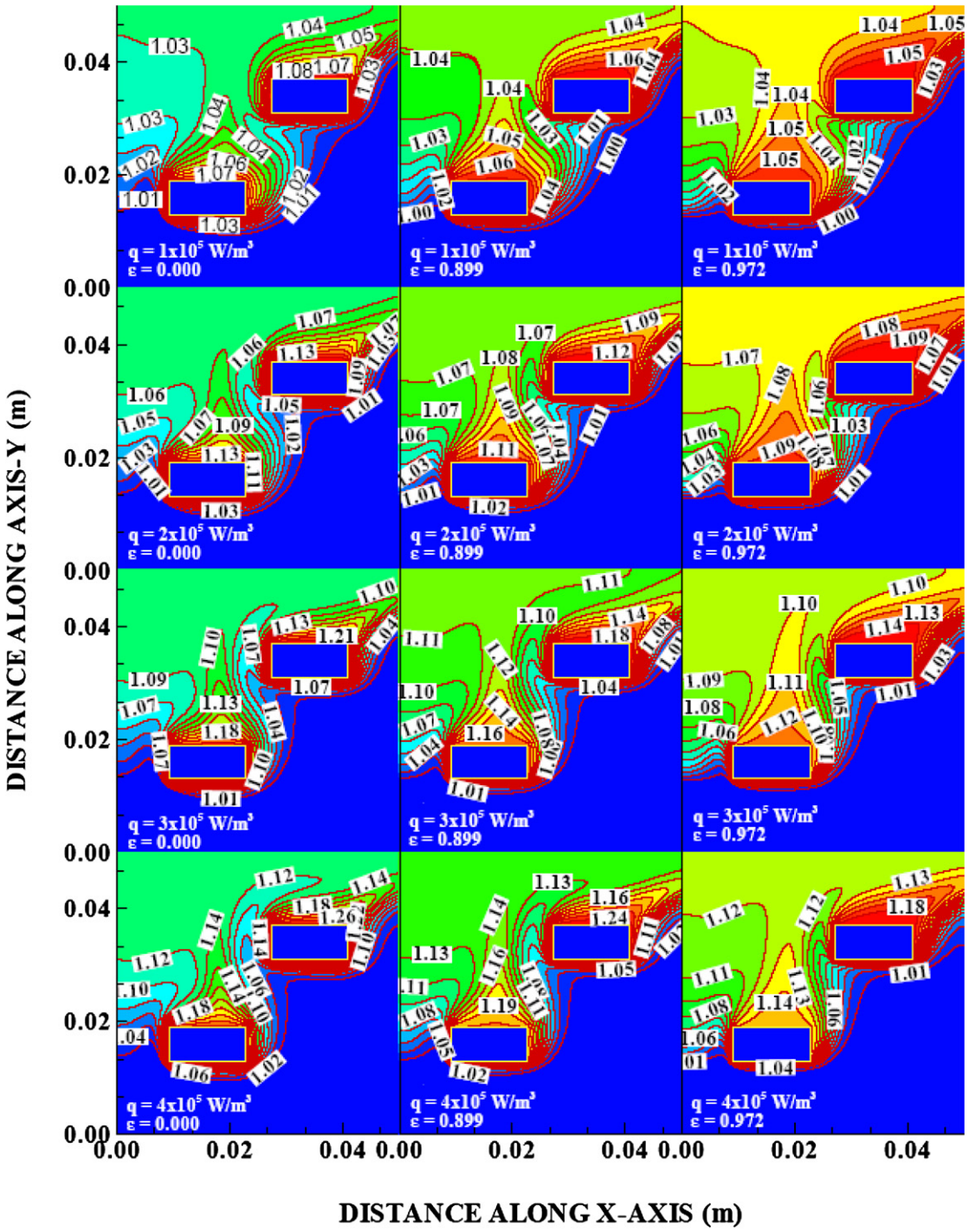

Fig. 4. Normalized temperature (T/T_i) contours in the cavity for different magnitude of heat flux and porosities.

the first block (Block 1). The reduction in the pressure coefficient is because of the fluid penetration into the block. Increasing the heat flux enhances the pressure coefficient due to extension of the high temperature field in the cavity. In this case, thermodynamic pressure contribution to the pressure coefficient becomes important, since the working fluid is air in the cavity. However, in all cases the pressure drop at the cavity exit is evident. The flow acceleration towards the cavity exit and frictional losses in the cavity are responsible for the pressure drop at the cavity exit. In the case of solid block, the pressure coefficient changes significantly in the region, where the flow acceleration is high. This is because of the blockage affect of the solid block in the cavity. In addition, the thermodynamic pressure contribution to the pressure rise becomes significant around the blocks, particularly in the region behind the blocks.

Fig. 6 shows the Nusselt number variation with the porosity for two blocks (Blocks 1 and 2, Fig. 1). The Nusselt number increases with increasing porosity. This is because of the flow penetration through the porous blocks; in which case, the forced convection current passing through the porous blocks enhances the cooling rates. In addition, the small thermal boundary layer around the porous blocks imposes temperature gradient in the vicinity of the blocks. This, also, enhances the conduction heat transport from the blocks to the working fluid. This situation occurs particularly for

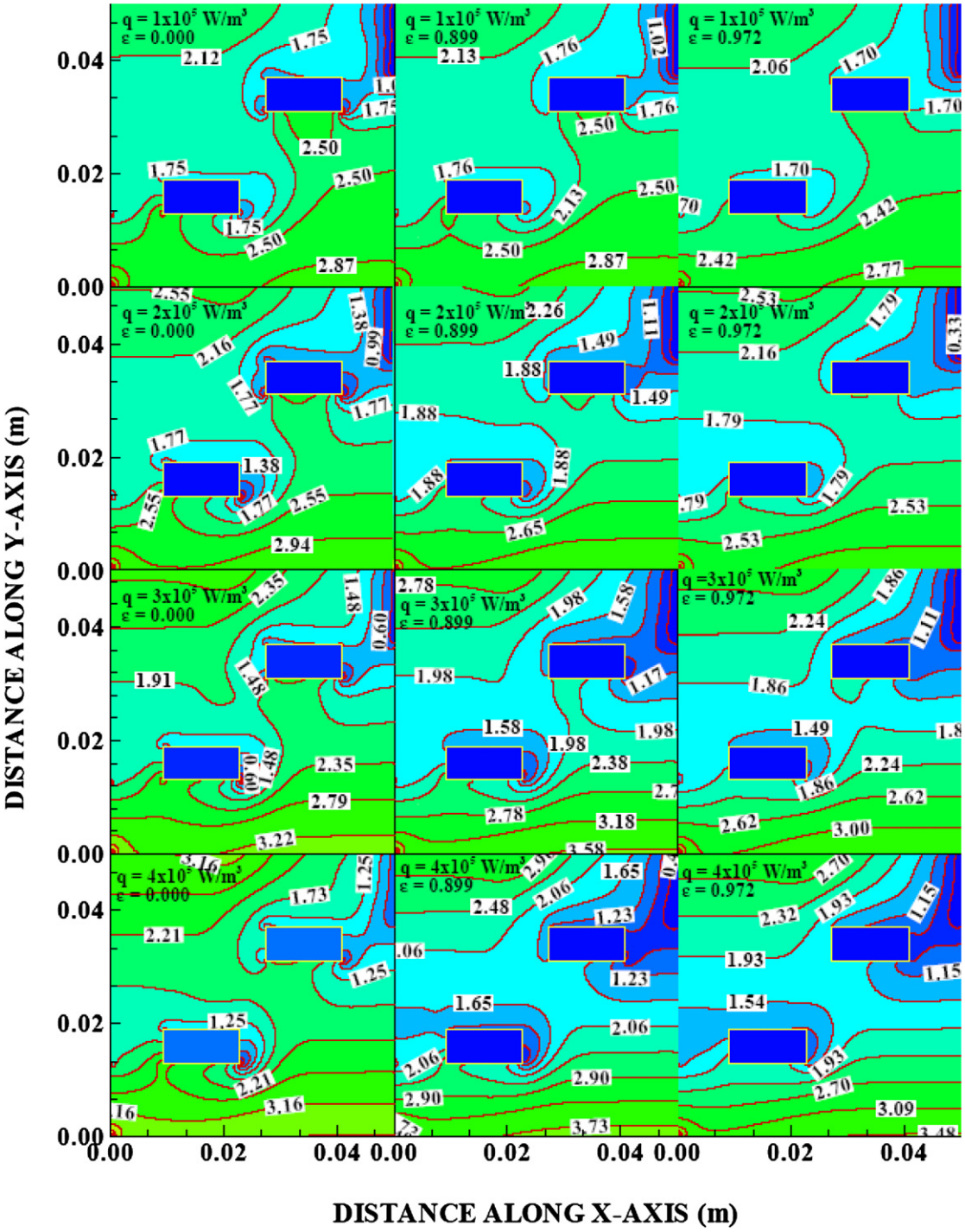

Fig. 5. Pressure coefficient contours in the cavity for different magnitude of heat flux and porosities.

high porosities. Increasing the heat flux increases temperature of the porous blocks. Since the cavity inlet temperature of the working fluid is constant, increasing heat flux increases the temperature gradient in the neighborhood of the blocks while enhancing the heat transfer from blocks to the working fluid. This improves the Nusselt number for both blocks. This situation is clearly observed for the high heat flux and the porosity. When comparing the Nusselt number corresponding to Blocks 1 and 2, Block 1 results in slightly high Nusselt number due to its orientation in the cavity, i.e., it is located close to the cavity inlet. Consequently, low temperature fluid entering into the cavity results in the high temperature gradient in the vicinity of the first block while enhancing the Nusselt number. The effect of block orientation on the Nusselt number is more pronounced at high porosities. In this case, the forced convection cooling of the first block through the fluid penetration contributes significantly to the enhancement of the Nusselt number.

Fig. 7 shows the Grashoff number variation with the porosity for two blocks and different heat fluxes. The Grashoff number decreases with increasing porosity; however, it increases with increasing the heat flux. Surface temperature of the porous blocks reduces with increasing porosity due to the enhancement in the heat transfer rates. Moreover, increase in the heat flux results in high temperature at the surface of the porous blocks enhanc-

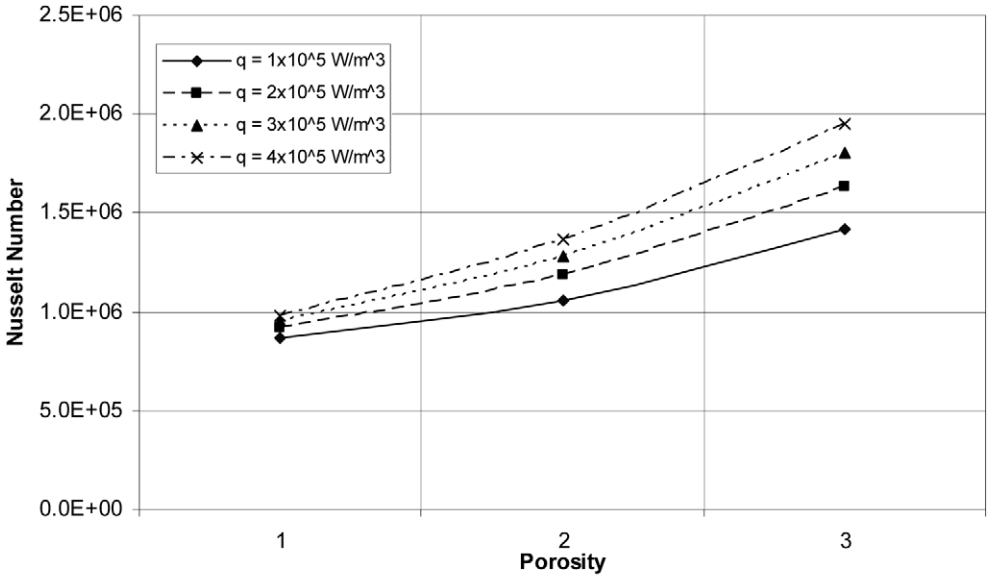

The Nusselt number variation with the porosity for Block 1.

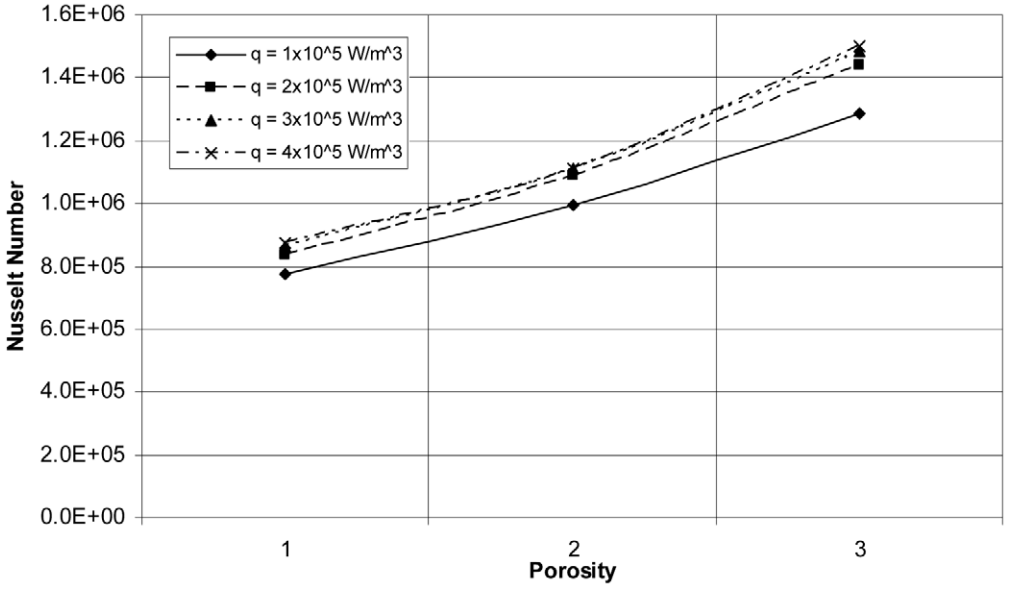

The Nusselt number variation with the porosity for Block 2.

Fig. 6. The Nusselt number variation with the porosity for two blocks in the cavity.

ing the Grashoff number. When comparing the Grashoff number for Blocks 1 and 2, the Grashoff number attains high values for Block 2. This is associated with the temperature field in the cavity and the surface temperature of the blocks. Consequently, enhancement in heat transfer reduces the Grashoff number while improving the Nusselt number around the blocks.

5. Conclusions

The flow structure and the heat transfer around the porous blocks situated in the square cavity are considered. The effects of the heat flux and the porosity on the heat transfer rates are examined. In the simulations, three porosities and four heat fluxes are accommodated and air is used as the working fluid. It is found that increasing porosity of the blocks modifies the flow field in the cavity and the flow emerging from the porous blocks contributes to the forced convection current. Increasing the heat flux influences the flow structure; in which case, the thermodynamic pressure and the natural convection current in the cavity become important. Enhancement of the Nusselt number with increasing porosity of the blocks is associated with the forced convection cooling of the porous blocks, which is more pronounced for the first block (Block 1). The heat flux influences the Nusselt number in such away that the Nusselt number increases with the increasing heat flux. This is because of the development of the high temperature gradient in the neighborhood of the blocks. When comparing the Nusselt number corresponding to the first and the second blocks, the Nusselt number attains values for the first block. This is because of the location of the first block in the cavity, which is close to the cavity inlet. The Grashoff number reduces with increasing porosity; however, it enhances with the increasing heat flux. This is more pronounced for the second block.

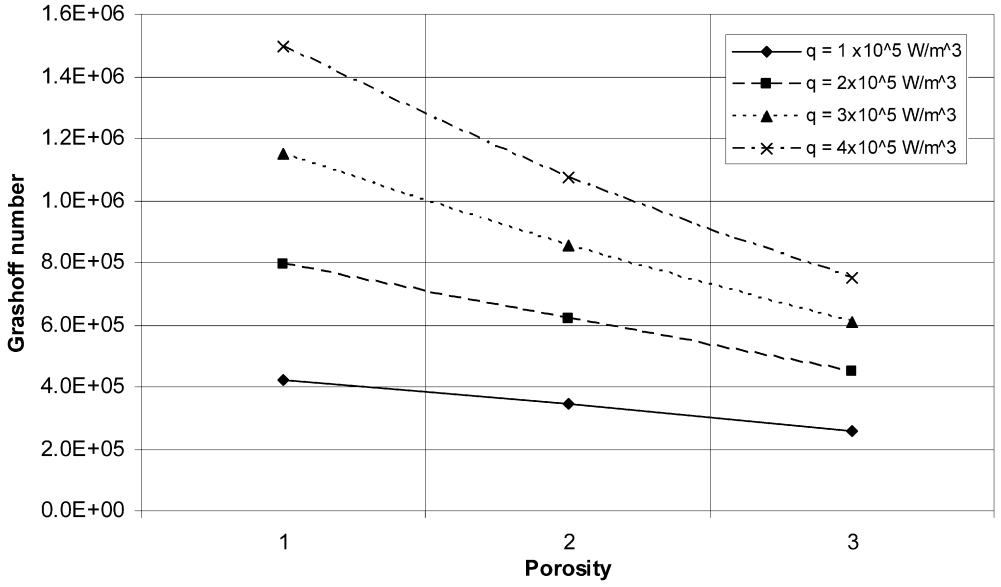

The Grashoff number variation with the porosity for Block 1.

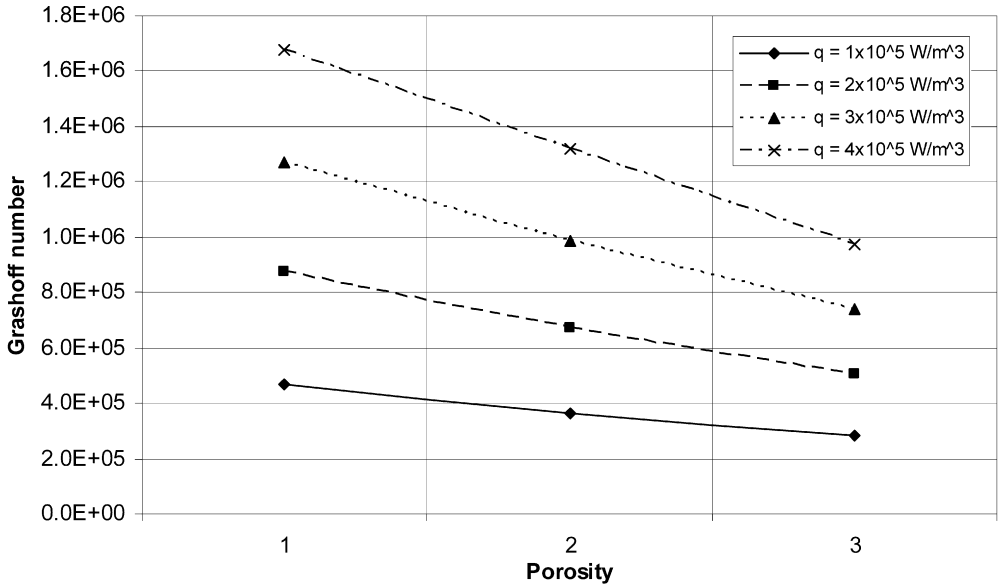

The Grashoff number variation with the porosity for Block 2.

Fig. 7. The Grashoff number variation with the porosity for two blocks in the cavity.

Acknowledgements

Acknowledgements are due to King Fahd University of Petroleum and Minerals.

References

[1] T.M. Jeng, S.C. Tzeng, Numerical study of confined slot jet impinging on porous metallic foam heat sink, International Journal of Heat and Mass Transfer 48 (2005) 4685–4694.
[2] I.A. Hassanien, F.S. Ibrahim, G.M. Omer, Unsteady flow and heat transfer of a viscous fluid in the stagnation region of a three-dimensional body embedded in a porous medium, Journal of Porous Media 9 (4) (2006) 357–372.
[3] H.L. Fu, K.C. Leong, X.Y. Huang, C.Y. Liu, An experimental study of heat transfer of a porous channel subjected to oscillating flow, ASME Journal of Heat Transfer 123 (2001) 162–170.
[4] Z. Vaszi, L. Elliott, D.B. Ingham, I. Pop, Conjugate free convection from a vertical plate fin with a rounded tip embedded in a porous medium, International Journal of Heat and Mass Transfer 47 (2004) 2785–2794.
[5] Q. Yu, A.G. Straatman, B.E. Thompson, Carbon-foam finned tubes in air–water heat exchangers, Applied Thermal Engineering 26 (2006) 131–143.
[6] H.Y. Zhang, D. Pinjala, Y.K. Joshi, T.N. Wong, K.C. Toh, M.K. Iyer, Fluid flow and heat transfer in liquid cooled foam heat sinks for electronic packages, IEEE Transactions on Components and Packaging Technologies 28 (2005) 272–280.
[7] M.S. Phanikumar, R.L. Mahajan, Non-Darcy natural convection in high porosity metal foam, International Journal of Heat and Mass Transfer 45 (2002) 3781–3793.
[8] K.C. Leong, L.W. Jin, Characteristics of oscillating flow through a channel filled with open-cell metal foam, International Journal of Heat and Fluid Flow 27 (2006) 144–153.
[9] S.V. Naidu, V.D. Rao, P.K. Sarma, T. Subrahmanyam, Performance of a circular fin in a cylindrical porous enclosure, International Communications in Heat and Mass Transfer 31 (2004) 1209–1218.
[10] J. Tian, T. Kim, T.J. Lu, H.P. Hodson, D.T. Queheillalt, D.J. Sypeck, H.N.G. Wadley, The effects of topology upon fluid-flow and heat-transfer within cellular copper structures, Int. J. Heat Mass Transfer 47 (2004) 3171–3186.
[11] N.B. Santos, M.J.S.D. Lemos, Flow and heat transfer in a parallel-plate channel with porous and solid baffles, Numerical Heat Transfer, Part A 49 (2006) 471–494.

[12] J.S. Coursey, J. Kim, P. Boudreaux, Performance of graphite foam evaporator for use in thermal management, J. of Electronic Packaging, ASME 127 (2) (2005) 127–134.

[13] A.G. Straatman, N.C. Gallego, B.E. Thompson, H. Hangan, Thermal characterization of porous carbon foam – convection in parallel flow, International Journal of Heat and Mass Transfer 49 (2006) 1991–1998.

[14] S.A. Khashan, A.M. Al-Amiri, I. Pop, Numerical simulation of natural convection heat transfer in a porous cavity heated from below using a non-Darcian and thermal non-equilibrium model, International Journal of Heat and Mass Transfer 49 (2006) 1039–1049.

[15] A. Battacharya, V.V. Calmidi, R.L. Mahajan, Thermophysical properties of high porosity metal foams, International Journal of Heat and Mass Transfer 45 (2002) 1017–1031.

[16] S.V. Patankar, Numerical Heat Transfer and Fluid Flow, Hemisphere Publishing Comp., Washington D.C., 1980.

[17] V.V. Calmidi, R.L. Mahajan, Forced convection in high porosity metal foams, ASME Journal of Heat Transfer 122 (2000) 557–565.